



PAPER

Preliminary engineering for *in situ in vivo* bioprinting: a novel micro bioprinting platform for *in situ in vivo* bioprinting at a gastric wound site

To cite this article: Wenxiang Zhao and Tao Xu 2020 *Biofabrication* **12** 045020

View the [article online](#) for updates and enhancements.


You may also like

- [Rheological and viscoelastic properties of collagens and their role in bioprinting by micro-extrusion](#)
Xiaoyi Lan, Adetola Adesida and Yaman Boluk
- [The emergence of 3D bioprinting in organ-on-chip systems](#)
Kirsten Fetah, Peyton Tebon, Marcus J Goudie et al.
- [Analysis of bioprinting strategies for skin diseases and injuries through structural and temporal dynamics: historical perspectives, research hotspots, and emerging trends](#)
Fei Teng, Wei Wang, Zhi-Qiang Wang et al.



PAPER

Preliminary engineering for *in situ in vivo* bioprinting: a novel micro bioprinting platform for *in situ in vivo* bioprinting at a gastric wound site

Wenxiang Zhao and Tao Xu 

Biomanufacturing Center, Department of Mechanical Engineering, Tsinghua University, Beijing 100084, People's Republic of China

E-mail: taoxu@mail.tsinghua.edu.cn**Keywords:** 3D cell printing, *in situ* bioprinting, tissue repair, gastric wound repair, hydrogels, Delta

Abstract

We first proposed the concept of *in situ in vivo* bioprinting in order to address the existing deficiencies in conventional bioprinting. Herein we verified this concept taking the case of the treatment for gastric wall injury and presented this work as a preliminary step towards a new method in the field of bioprinting. In this study, a micro bioprinting platform which can be installed to an endoscope was developed to enter the human body and process bioprinting. Printed circuit micro-electro-mechanical-system techniques were used in the design and fabrication of the platform. Control system with high accuracy was developed and performance tests were carried out to verify the feasibility of the platform. The 2-layer tissue scaffolds were printed in a stomach model. Gelatin–alginate hydrogels with human gastric epithelial cells and human gastric smooth muscle cells were used as bioinks to mimic the anatomical structure of a stomach. A 10 d cell culture showed that printed cells remained a high viability and a steady proliferation, which indicated good biological function of cells in printed tissue scaffolds. This work presents an innovative advance not only in the field of bioprinting but also in the clinical sciences.

1. Introduction

Bioprinting technologies have been greatly developed in recent decades with the combination of automation, digitalization and new tissue engineering approaches. It refers to fabrication of scaffolds by additive manufacturing technology, which deposits bioinks layer by layer as designed and construct tissues or organs with biological functions and activities [1, 2]. This technology has been applied to plenty of fields such as regenerative medicine, disease modeling and drug screening etc [3–6]. As a new branch of bioprinting, *in situ* bioprinting was proposed based on inkjet bioprinting in 2007 [7]. It refers to a method that bioinks are directly printed at a defect site in a clinical setting to create or repair living tissues or organs [8]. *In situ* bioprinting has developed rapidly in recent years and various studies have shown the great potentials of this approach, in fields such as skin, bone and cartilage repair [9–12]. This emerging technology may doubtless bring a breakthrough in bioprinting for clinical application. However, most of the current studies relating *in situ* bioprinting target the repair of defects in outer tissues, while there

still exists potential demand for repair in inner tissues such as digestive tract or genital tract. Unfortunately, former studies showed that the existing setups for *in situ* bioprinting are normally large, thus they are not able to be applied to inner tissue repair as well as may cause secondary impact while performing *in situ* bioprinting through incisions so as to give enough room for printing operation. To address this need, we have proposed the new concept of *in situ in vivo* bioprinting for the first time, aiming to create a micro robot to enter the human body noninvasively and carry out tissue repair inside the body. This paper will expound this concept in detail taking the case of the treatment for gastric wall injury.

Gastric wall injury is one of the most common diseases in digestive tract and about 12% of the world's population suffer from it to varying degrees, according to a research of Lancet [13]. Recent studies have showed that the main reason for common gastric wall injury is *H. pylori* inside digestive tract weakened protective effects of mucosae. And the mainstream treatment methods includes conservative medication and surgical treatments. Though these methods are therapeutic in some degree, medication take effect

slow, has poor target and is easy to relapse. Surgical treatments mainly remove focuses in gastric tract physically, which can increase discomfort and the risk of complications [14]. Minimally invasive surgery through an endoscope, which was presented in recent years, also exist limitations: suturing wound under endoscope with LAPRO-CLIP can only mend small damage limited to narrow spaces in natural orifices [15]. Spraying colloid styptic by endoscope to a wound can stop bleeding effectively but cannot reconstruct 3D structure of the wound. Therefore, it is necessary to explore new method in treatments for gastric wall injury, such as introducing bioprinting techniques to tissues repair, creating organized 3D tissue constructs through layer-by-layer assembly to repair defects inside the stomach.

At present, little research has been carried out on the application of bioprinting techniques to tissue repair in gastric tract, yet this is a field worth exploring. To carry out bioprinting *in situ in vivo*, the first step is to develop an available micro bioprinter, based on which we can continue subsequent research on creating tissues with bioactivities. This paper is the first step of the research on a new approach aiming to repair tissues through *in situ in vivo* bioprinting. We developed a micro 3D bioprinting platform which can be installed to an endoscope and can reach designated spot to carry out *in situ* 3D printing. The schematic of this process is shown in figure 1. The development of the micro bioprinter proposes the brand new concept of *in situ in vivo* bioprinting and provides a new idea in the diagnosis and treatment for gastric wall injuries.

Herein we introduced the design principles, fabrication, and performance and biological testing of the first prototype device in our preliminary research. The device was designed and fabricated in the concept of printed circuit micro-electro-mechanical-systems (PC-MEMS) [16, 17], and it was controlled accurately by mathematical calculation and programming. The accuracy and workspace were acquired through experiments and simulation, indicating this platform's feasibility in bioprinting. Furthermore, our preliminary biological experiments using this device to print hydrogel structures demonstrates the capacity of the device for *in situ in vivo* fabrication of 3D tissue scaffolds as well as the application prospect in clinical field.

2. Materials and methods

2.1. Design principles

Our objectives in this work were to create a sub-miniature bioprinting platform which is capable of entering human's body and proceeding bioprinting with hydrogels and living at high viability to construct tissue scaffolds. Besides, the projection of the platform's working space should be larger than the platform's cross-sectional area, so that the platform

can achieve as much workspace as possible within as little space as possible. In order to meet these principles, construction of Delta robot was used as the basic structure of the platform shown in figure 2(A), which can fold into a small state when entering into the patients' body and unfold before working (figure 2(B)). Besides, we used PC-MEMS for reference to make the miniaturization of the platform possible. The conventional Delta robot consists of two parallel flats: the fixed base and the moving platform, which are connected by three kinematic chains [18]. Each kinematic chain is composed of a driving arm and a passive arm, which are connected by spherical hinge. The latter one consists of a parallelogram closed loop to keep the moving platform moving horizontally. However, a spherical hinge is too difficult to process in such a micro platform so we used PC-MEMS techniques to create two perpendicular revolving joints composed of two rigid layers and one flexible layer with offset axes of rotation to replace the original spherical hinge in the kinematic chains.

2.2. Control and simulation

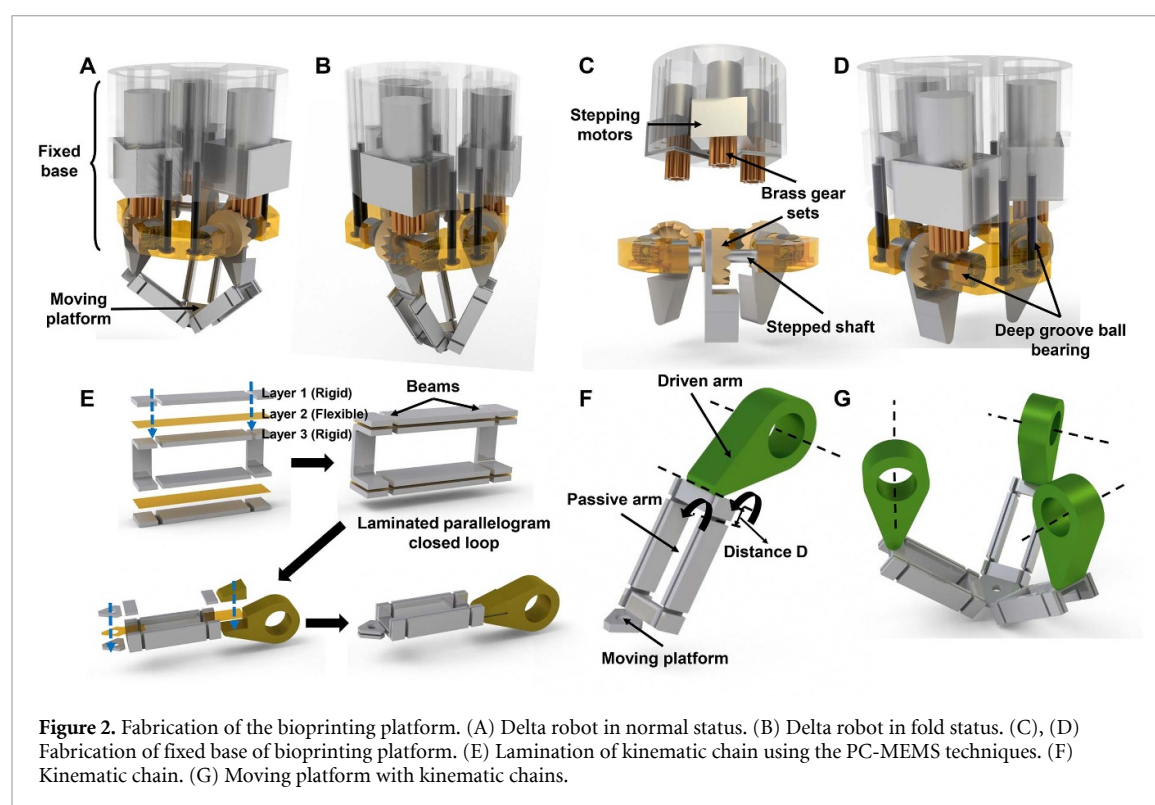
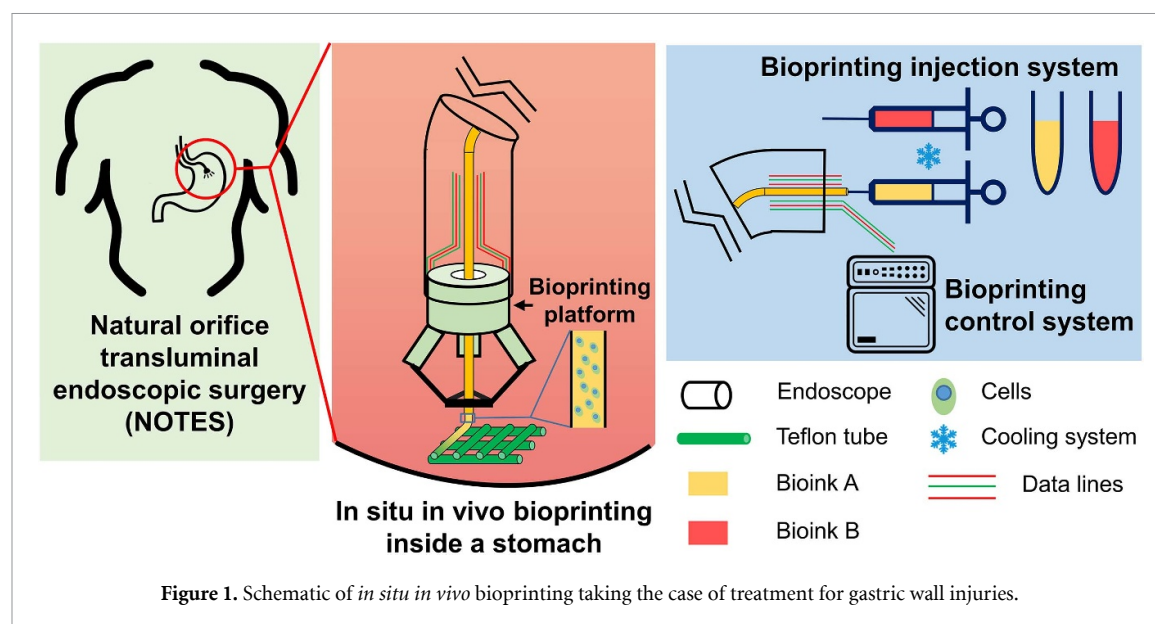
The overall frame of the bioprinting platform is a Delta robot, which is composed of a fixed base, moving platform and three identical kinematic chains. Thus, the control and simulation of the conventional Delta robot can be used for reference in this part [19–21]. First, a basic mathematical model was abstracted from the platform and the mathematic relation between the Cartesian position of the center of the moving platform and each actuators' deflections was derived, which was the foundation of bioprinting. On the basis of mathematic relation, interpolation algorithm [22] was applied to constitute the kinematic model, which made it possible that the platform carries out printing according to trajectory. The workspace of bioprinting platform can be derived from the relation mentioned above as well [23], and it was expressed by MATLAB directly as a reference to bioprinting feasibility.

2.3. Bioprinting performance test

To test the platform's ability in bioprinting, it should perform the basic trajectories necessary in tissue scaffolds such as latticed structure and planar circle. The kinematic model was used to generate input signals for the trajectories, and the platform's output motions were captured by a laser tracker. The deviation of the platform can be acquired through the comparison between input and output trajectories.

2.4. Preparation of bioinks for bioprinting

Gelatin (type A from porcine skin, Sigma-Aldrich, G1890) and alginic acid sodium salt power (Sigma-Aldrich, A0682) were dissolved in 0.9% sodium chloride solution with a concentration of 10% (w/v)



gelatin and 4% (w/v) alginate as storage bioink solutions. The bioink solutions were sterilized by heating at 70 °C for 30 min three times, and then stored in 4 °C before usage. Calcium chloride (Beijing Chemical Works, Beijing, China) granules were dissolved in deionized water to make 3% (w/v) solutions. Solutions were filtered with 0.22 μm PES Syringe Filter (Membrane Solutions).

2.5. Cell preparation for bioprinting

To mimic the structure of gastric ulcers [24], human gastric epithelial cells (GES-1 cells) and human gastric smooth muscle cells (HGSMCs) (Otto Biotech

(Shenzhen) Inc. Shenzhen, China) were used in this study. These cells were cultured in RPMI Medium 1640 (Thermo Fisher Scientific), supplied with 10% fetal bovine serum (Biological Industries) and 1% penicillin G and streptomycin (Gibco, 10378–016). Cells were cultured in an incubator at 37 °C in 5% CO_2 and passaged every 3 d. After achieving about 80% confluence, cells were harvested with 0.25% trypsin/EDTA dissociation at a density of 3×10^6 cells ml^{-1} separately. Then the rewarmed bioink and the cell suspension were mixed at a volume ratio of 1:1. Bioink A was composed of 5% gelatin, 2% sodium alginate and GES-1 cells with a density of

1.5×10^6 cells ml^{-1} and Bioink B was composed of the same concentration of HGSMCs.

2.6. Experimental setup

The stomach model in the experiment was obtained from the reconstruction of a human CT data in MIM-ICS (MIMICS Research 20.0, Materialise, Belgium) and it was fabricated through stereolithography using transparent resin (WeNext Inc. Shenzhen, China). A curved pipe was also fabricated through stereolithography using transparent resin (WeNext Inc. Shenzhen, China) to mimic an endoscope. The bioprinting platform was fixed on the endoscope and there was a 23 gauge needle installed in the moving platform and connected to a syringe through a polytetrafluoroethylene (PTFE) tube to reduce friction during the extrusion of bioinks. The endoscope with bioprinting platform entered the stomach model to perform bioprinting. In order to carry out subsequent biological test, bioprinting was performed in a 35 mm cell culture dish rather than the inner surface of the stomach model to mimic gastric ulcer injury repair. The formal experiment was carried out in a clean bench in order to obtain a sterile printing environment. Before printing, the bioprinting platform, the endoscope, the PTFE tube and the stomach model were wiped with 75% ethanol 3 times and transferred to a clean bench for ultraviolet (UV) light treatment for 2 h.

2.7. Tissue scaffolds bioprinting

The bioprinting process of tissue scaffolds was divided into two parts: the formation of a 2-layer lattice structure and crosslinking by CaCl_2 . Before printing, syringe containing bioinks were pre-cold in 4 °C refrigerator for 3 min. Next, the syringe with Bioink B (containing HGSMCs) was connected to the bioprinting platform through a 300 mm-long PTFE tube and extruded by a double-channel syringe pump at a speed of 0.05 ml min^{-1} . Meanwhile, the platform preformed the lattice structure's printing. After the first layer was accomplished, another syringe with Bioink A (containing GES-1 cells) replaced the first syringe quickly and the platform printed the second layer right above the first layer. After the 2-layer lattice structure was printed, a syringe containing CaCl_2 replaced the former syringe and the platform repeated the lattice trajectory, delivering cross-linking agent CaCl_2 to the tissue scaffolds and chemically cross-linking for 3 min. Because there was residual bioink in the PTFE tube, the timing was optimized to make sure that each layer only contained one kind of cells. In this structure, GES-1 cells were in the upper layer and HGSMCs in the lower layer, which simulated the gastric wall's structure with gastric mucosa on the outside and muscle layer inside [24]. Then the cell culture dish was taken out, CaCl_2 was replaced with 2 ml cell culture media and then the dish was transferred to an incubator at 37 °C with 5% CO_2 for 10 d.

To observe the cell distribution after bioprinting, GES-1 cells and HGSMCs were respectively stained with 5-chloromethylfluorescein diacetate (CM-FDA) and $\text{C}_{42}\text{H}_{40}\text{ClN}_3\text{O}_4$ (CM-TPX) (Thermo Fisher Scientific) when harvested. CM-FDA and CM-TPX are living cell trackers with high stability and low cell-specificity, which infiltrate cell membranes and react with intracellular components to form a fluorescence that remains for at least 72 h. GES-1 cells were stained green and HGSMCs were stained red. The samples were observed under a laser scanning confocal microscope (LSCM) (ZEISS).

2.8. Cell viability assay upon bioprinting

Cell viability assay was performed immediately after bioprinting to evaluate cell survival by the effect of the shear force of the nozzle. On days 3, 7 and 10, the viability assay was performed as well. In this assay, calcium acetoxymethylester (calcein-AM) (Sigma) and propidium iodide (PI) (Sigma) were used as LIVE/DEAD assay reagents. Calcein-AM is metabolized by live cells to form green fluorescence. PI can pass through dead cell membranes and stain the DNA to produce red fluorescence.

Staining solutions were prepared following the instructions. Briefly, 1 mg Calcein-AM was dissolved in 1 ml anhydrous dimethylsulfoxide (DMSO) (Sigma) and 1 mg PI was dissolved in 1 ml sterile water to make staining solutions. 2 μl Calcein-AM staining solution and 3 μl PI staining solutions were added into 1 ml sterile phosphate buffer solution (PBS) (Biological Industries) and fully mixed. One printed sample was gently washed with PBS and incubated with 1 ml staining solutions for 15 min at room temperature in the dark. After incubation, the structure was gently washed with PBS and observed under a LSCM. Three random fields were captured and cell viability was calculated by counting cells using the software Image-J.

2.9. Cell proliferation

On culture days 0, 3, 7 and 10, printed structures were incubated with a mixture of culture medium and cell counting kit-8 (CCK-8) (Yeasen, Shanghai, China) at a volume ratio of 10:1 to investigate cell proliferation. After 1 h incubation at 37 °C, the absorbance of formazan dye was determined at 450 nm using a Microplate Reader (Thermo Fisher Scientific). The obtained data was normalized to the cell number according to the pre-established standard curve. Three samples were tested in each time point.

2.10. Statistical analysis

Statistical analysis was performed by Origin 2018 using two-way analysis of variance (ANOVA) in conjunction with a Bonferroni *post-hoc* test and Stu-

dent t-test. Differences were considered statistically significant when p-values were lower than 0.05. Three independent trials were carried out unless otherwise stated.

3. Results and discussion

3.1. Fabrication of bioprinting platform

Figure 2(E) shows the basic lamination and folding steps of one kinematic chain. We used aluminum alloy with a thickness of 0.5 mm as rigid layers (Layer1 and Layer3) for its high stiffness and strength and polyimide film with thickness of 100 μm as flexible layer (Layer2) for its flexibility and favorable mechanical properties. Among them, aluminum alloy plates were processed by laser to their expected shape. After that, Layer1 and Layer3 were solidified to Layer2 through adhesive epoxy on the surface of the flexible layer. In the process of solidification, there exist beams between adjacent rigid plates where deflection occurred. When deflection occurred in the beam, the rigid layers offered an effective support. The width of beams should be strictly equal to the thickness of 2 rigid layers, i.e. 1 mm. Because a wider beam means less support which will lead to the uncontrollable deflection, while a narrower beam will restrict range of deflection. A laminated parallelogram closed loop can be acquired through the steps mentioned above, which was able to revolve around the axis showed in figure 2(F). While the loop only had one degree of freedom, the same method was used to connect the parallelogram closed loop to the moving platform and the driven arm, which composed the laminated kinematic chain.

After the lamination of the frame and the mechanism structure which consists of three kinematic chains, the resulting laminates were manually assembled with components for actuation. Stepping motors (AM0820) were used as actuators for their tiny sizes with 8 mm in diameter. Gear reduction with reduction ratio of 75:1 was used, raising the driving torque to 4.87 N · cm and the step angle to 0.24°, enabling highly accurate control of the hardware. Meanwhile, to decrease friction between the shaft and the bracket, deep groove ball bearings (618/2) were used and shaftings were designed. Figure 2(C) shows the designed stepped shaft to locate gears and bearings. In addition, all the components were attached to a 3D-printed bracket as fixed frame and the final diameter of the micro bioprinter was 30 mm. The length of it was from 43 mm to 59 mm, which depends on the state of the bioprinting platform shown in figures 2(A) and (B).

3.2. Kinematic modeling and workspace simulation

The 3D bioprinting platform used the Delta robot as its basic structure, which was composed of a fixed base, moving platform and three identical kinematic chains. In the abstracted model shown in figure 3(A),

both the base and moving platform were regular triangles. The circumradius of the fixed base was defined as R , the circumradius of the moving platform was defined as r , the length of the driven arm B_iE_i was L_1 and the length of the passive arm P_iE_i (parallelogram closed loop) was L_2 . To simplify the model, the passive arm containing 4 spherical hinges was abstracted to a virtual rod with 2 hinges. The nodes E_i can be presented in the coordinate system O - XYZ attached to the fixed base, and the nodes P_i can be presented in the coordinate system O' - $X'Y'Z'$ connected to the moving platform. ($i = 1, 2, 3$)

$${}^O E_i = \begin{bmatrix} (R + L_1 \cos \theta_i) \cos \alpha_i \\ (R + L_1 \cos \theta_i) \sin \alpha_i \\ -L_1 \sin \theta_i \end{bmatrix} \quad {}^{O'} P_i = \begin{bmatrix} r \cos \alpha_i \\ r \sin \alpha_i \\ 0 \end{bmatrix} \quad (1)$$

Where $\alpha_i = (\frac{2}{3}i - \frac{1}{2})\pi$ ($i = 1, 2, 3$)

Using the length of the passive arm, the relationship between the position of the center of the moving platform and each actuator's deflections can be derived from:

$$L_2 = |{}^O E_i - {}^{O'} P_i| \quad (2)$$

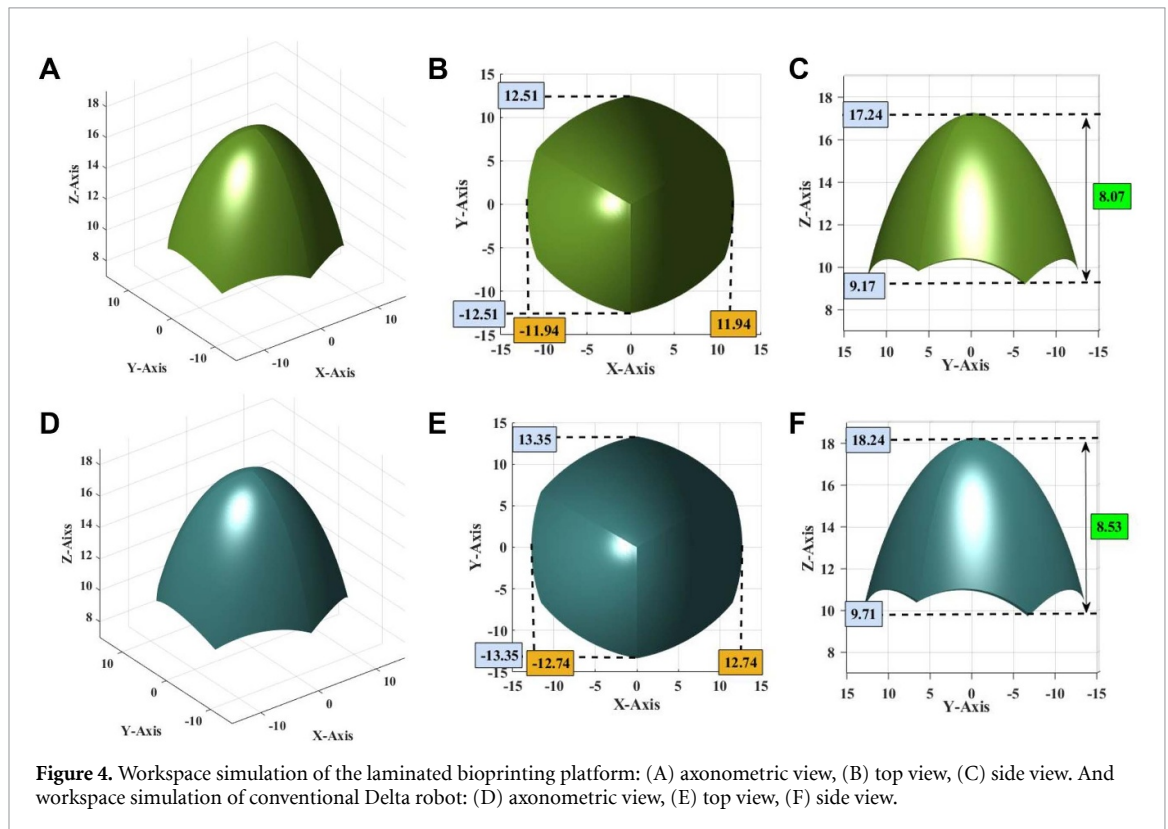
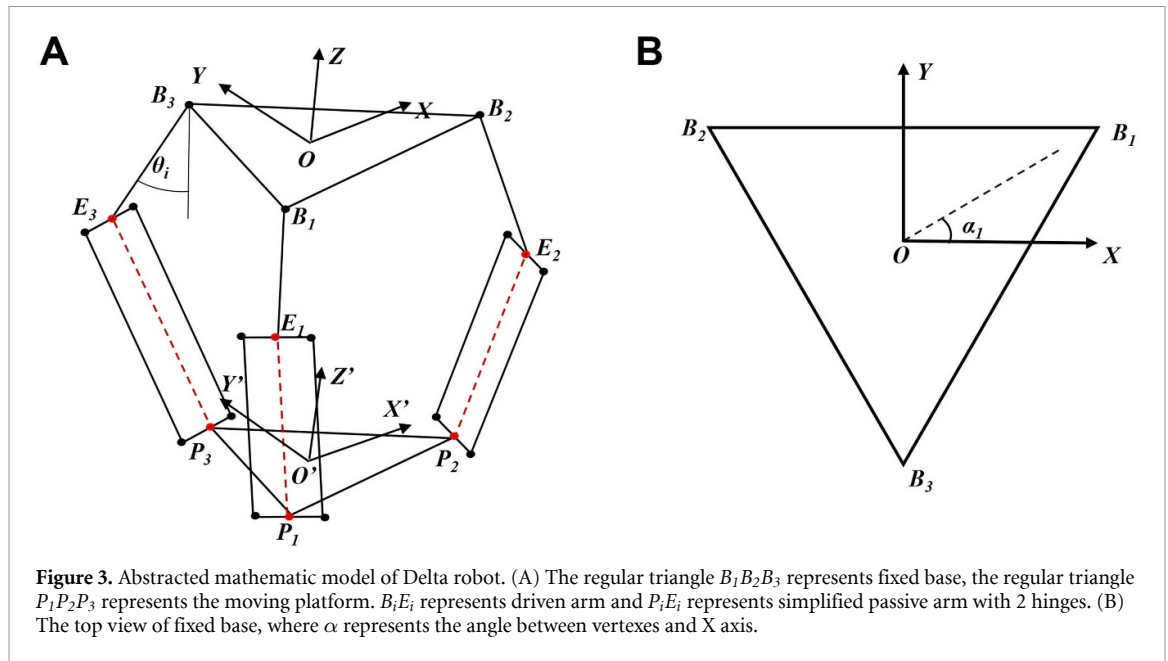
Substituting equation (1) to equation (2), it becomes:

$$L_2^2 = [(R + L_1 \cos \theta_i - r) \cos \alpha_i - x_i]^2 + [(R + L_1 \cos \theta_i - r) \sin \alpha_i - y_i]^2 + (L_1 \sin \theta_i + z_i)^2 \quad (3)$$

The inputs for forward kinematics were the actuator deflections θ_i , and the outputs were the Cartesian position of the center of the moving platform. For the inverse kinematics, a 3-DOF Cartesian joint between the center of the moving platform and world frame was used to input different trajectories, and the linearized actuator deflections were recorded as outputs correspondingly.

The bioprinting platform's workspace can also be derived from equation (3) and we performed a simulation study using the kinematic model described above. Figure 4 shows the workspace of laminated bioprinting platform compared with the workspace of a conventional Delta robot.

The distance between the rotational axes of the laminated universal joints D shown in figure 2(F) will affect the workspace to a certain extent, thus the distance D cannot be large. In this case, D was 2 mm, making the workspace's deviation 7% compared with a traditional Delta robot. Besides, the maximum cross-sectional area of the laminated workspace was 462.8 mm², which was basically the same as the platform itself and met the design objective above to some extent.



3.3. Performance test of bioprinting platform

The output motion trial was captured by a laser tracker, and its comparison with the input trajectory is shown in figure 5. The captured output motion was in the form of Cartesian coordinates of a series of dots on the output motion trajectory. Taking the geometric center as origin of coordinates, the coordinates of dot i were $P_i (x_i, y_i, z_i)$. The coordinates of corresponding dot on input trajectory were $P_{0i} (x_{0i}, y_{0i}, z_{0i})$, then the deviation dP can be defined as

$$dP = |P_i - P_{0i}|$$

After three independent experiments, the average deviation in latticed structure with a side dimension of 14 mm was $1.18 \text{ mm} \pm 0.43 \text{ mm}$. While the deviation in planar circle with a radius 10 mm was $0.67 \text{ mm} \pm 0.15 \text{ mm}$. It can be seen from figure 5(B) that the biggest deviation appeared at the corners of latticed structure for these positions were close to the boundary of working space. If the four corners of the latticed structure were removed, the average deviation dropped down to $0.62 \text{ mm} \pm 0.13 \text{ mm}$, which is

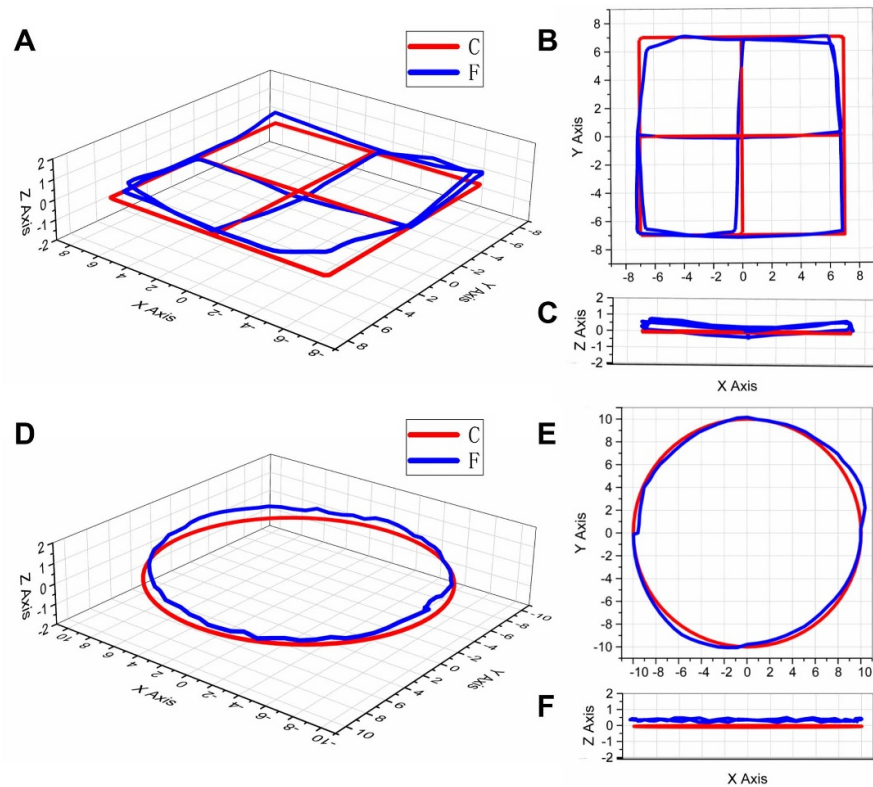


Figure 5. Comparison between input trajectory and output motion. Latticed structure: (A) axonometric view, (B) top view, (C) side view. Planner circle structure: (D) axonometric view, (E) top view, (F) side view ((C): input trajectory; (F): output motion).

an improvement from the former value. This implies that the moving platform should avoid approaching edges of working space during bioprinting for achieving higher accuracy. These values demonstrated the bioprinting platform's ability to perform the basic trajectories necessary in tissues scaffolds in bioprinting. More generally, it illustrated that mechanisms found in conventional Delta robots can be microminiaturized by using laminate design and PC-MEMS techniques and this can make *in situ in vivo* bioprinting a reality.

Figure 6 shows the bioprinting process inside the stomach model. The printed 2-layer structure consisting of GES-1 cells and HGSMCs before cross-linking is shown in figure 6(C). It can be seen that this structure was stable and its printed fibers were smooth with an average thread diameter of $500\ \mu\text{m}$. The 2-layer structure can maintain its cell culture stably for 10 d, making it possible for subsequent biological experiments. To demonstrate the printing performance of the bioprinter, an 8-layer lattice structure was printed onto a glass-slide with an overall thickness of 3 mm. After cross-linking, the 8-layer scaffold showed high shape fidelity, clear contours as well as favorable mechanical properties and can be picked up by a tweezer.

3.4. Cell distribution in tissue scaffolds

After cell distribution analysis, an image of stained cells was obtained with a LSM. GES-1 cells were

stained green and HGSMCs were stained red. It can be seen in figure 7(A) that HGSMCs are distributed in the lower layer and GES-1 cells are distributed in the upper layer, which mimics the anatomical structure of gastric wall. Figure 7(B) shows side views of the stained structure. It can be seen that the boundary of the 2 layers was clear and the thickness of each layer was around $350\ \mu\text{m}$, which proved that layers of the tissue scaffolds were kept in good condition after *in situ in vivo* bioprinting.

3.5. Cell viability upon bioprinting

Figure 8(A) shows the results of a 10 d cell-viability assay, which were obtained with a LSM. The image revealed that most of the cells were viable (green) after *in situ in vivo* bioprinting. The average cell viability reached $94.3\% \pm 2.2\%$, which proves that the cells distributed in 2-layer tissue scaffolds live well. It can also be seen from figure 8(B) that the viability of cells was high in the first 7 d, while it showed a slight downward trend after day 7. It was probably caused by the proliferation of the cells. When the scaffolds were filled with cells, with their proliferation and changes in morphology, lacking growing space would lead to decline of cells' viability. In addition, both GES-1 cells and HGSMCs were spindle-like or rhomboid [25], so the cell spreading would accelerate the competition for growing space. Even so, viability of the cells still remained above 90%, which showed

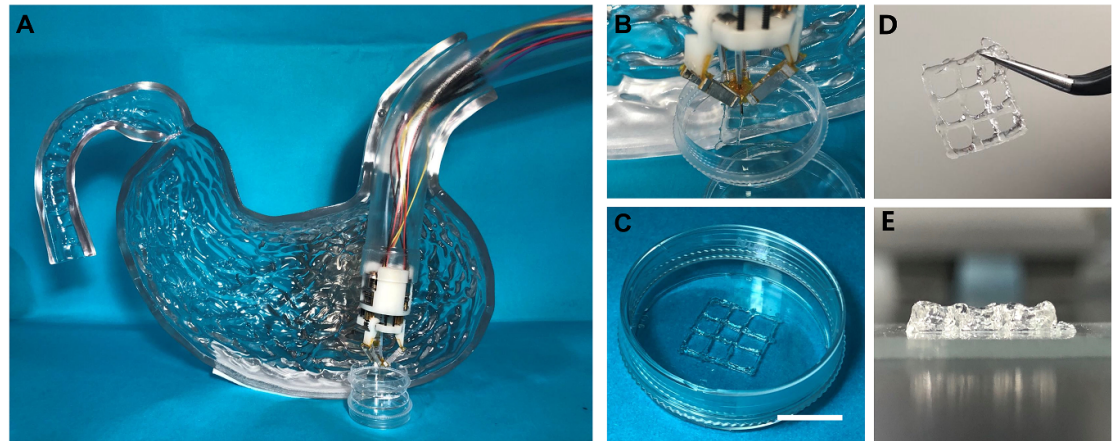


Figure 6. Bioprinting experiment equipment. (A) Bioprinting platform installed to a curved pipe mimicked an endoscope to process bioprinting inside a model of stomach. (B) The process of *in situ in vivo* bioprinting. (C) The printed 2-layer tissue scaffolds consisting of GES-1 cells and HGSMCs before cross-linking. (Scale bar: 1 cm). (D, E) The printed 8-layer scaffold with favorable mechanical properties.

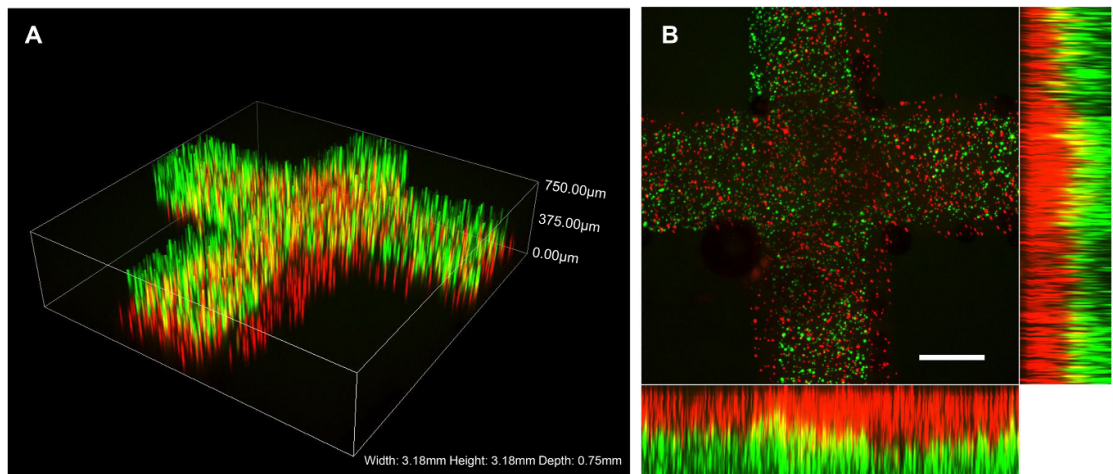


Figure 7. (A) 3D reconstructive image of the 2-layer structure showing the distribution of the printed cells. (GES-1 cells were stained green and HGSMCs were stained red). (B) Top view and side view of the stained structure showing the boundary of the 2 layers (Scale bar: 500 μm).

that the cells could maintain a good viability after bioprinting, proving the feasibility of this method.

3.6. Cell proliferation and morphology observation

The bioprinted 2-layer tissue scaffolds were cultured in an incubator for 10 d. During the culture, cell proliferation was investigated through CCK-8 mentioned above and cellular morphological changes were observed. Figure 9(B) shows the diagram of cell proliferation during the culture period and it can be seen that compared with day 0, the cells showed significant proliferation. The day 10 data showed 2.1-fold proliferation compared with that on day 0, which indicated that cells had great proliferative function in the bioprinting tissue scaffolds.

Morphological changes of cells in the bioprinted structure were observed under a light microscope and pictures of the structure on days 0, 3, 7

and 10 were captured and are shown in figure 9(A). The cells remained spherical on day 0 and gradually became spindle-like or rhomboid with cell spreading in day 3. With cell proliferation, the number of cells grew as well which can be seen clearly on days 7 and 10. These results matched well with the proliferation experiment mentioned above and proved that the collagen–alginate system could benefit the viability and proliferation of cells.

4. Discussion

In situ in vivo bioprinting is a brand new research direction in biofabrication, which determines there are plenty of exploration to work with. As the preliminary research of the systematic exploration, this paper has some merits, but also exists room for improvement.

In the development of micro bioprinting platform, the delta construction was used as the basic

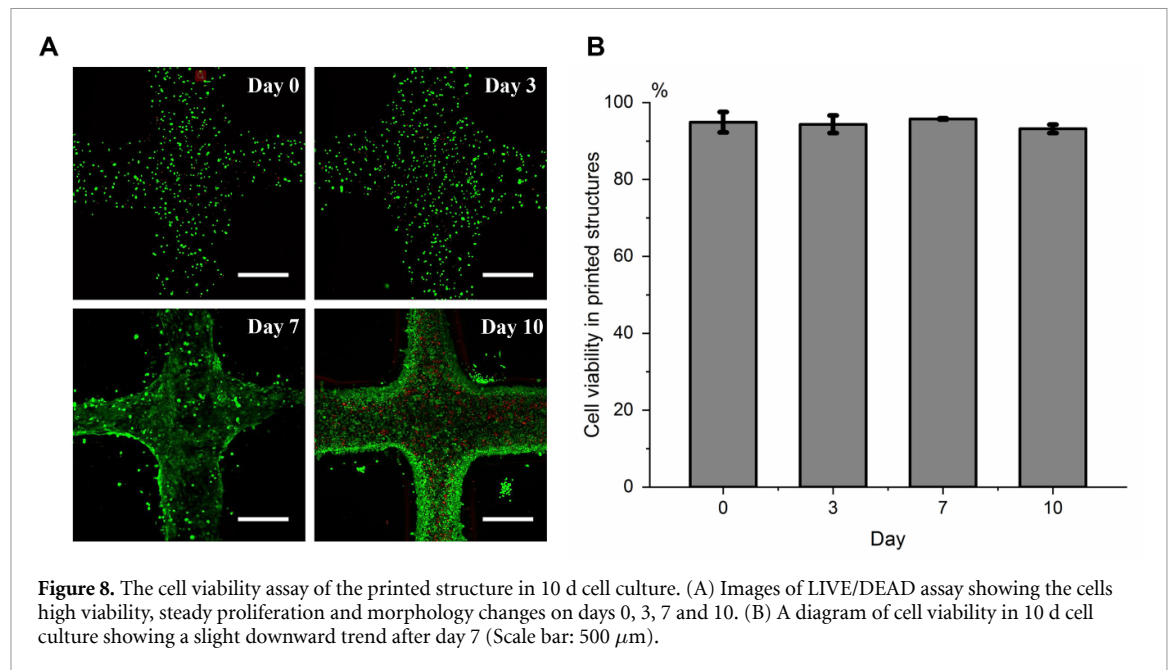


Figure 8. The cell viability assay of the printed structure in 10 d cell culture. (A) Images of LIVE/DEAD assay showing the cells high viability, steady proliferation and morphology changes on days 0, 3, 7 and 10. (B) A diagram of cell viability in 10 d cell culture showing a slight downward trend after day 7 (Scale bar: 500 μm).

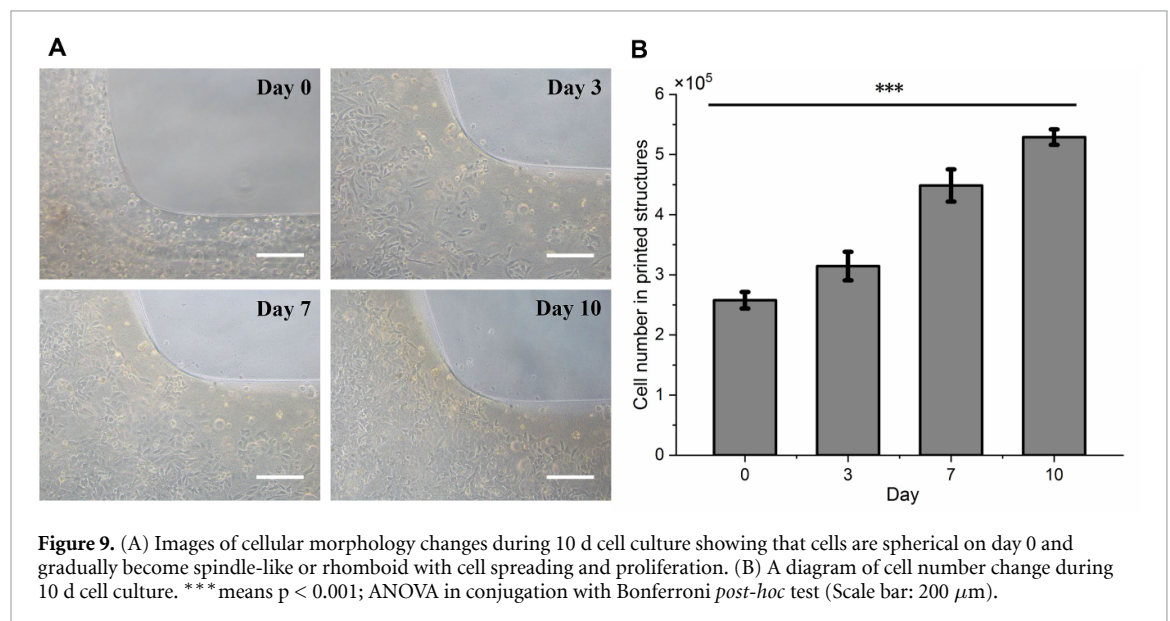


Figure 9. (A) Images of cellular morphology changes during 10 d cell culture showing that cells are spherical on day 0 and gradually become spindle-like or rhomboid with cell spreading and proliferation. (B) A diagram of cell number change during 10 d cell culture. *** means $p < 0.001$; ANOVA in conjugation with Bonferroni *post-hoc* test (Scale bar: 200 μm).

structure due to its faster travel speed and more compact size relative to typical gantry-like system. The utilization of PC-MEMS technique makes it possible for microminiaturization of delta construction, which makes it a columnar printer with diameter 30 mm. Compared with conventional bioprinter, it is indeed a micro printer. While we aim to install the bioprinter on the endoscope to enter the human body through the natural orifice and process 3D printing. According to a review of endoscopy [26], the existing flexible therapeutic endoscopes are from 16 mm to 20 mm in diameter, compared with which, the micro bioprinting platform is a bit bigger than the existing endoscopes. In response to this issue, it should be clarified that further microminiaturization of the bioprinter is feasible. The bioprinting platform mainly consists

of two parts, a laminated moving platform fabricated by PC-MEMS technique as well as a fixed base containing three actuators. PC-MEMS technique had been applied in designing and manufacturing of micro-robot since its development in 2012. Modern micromachining techniques cooperated with PC-MEMS, allowing the manufacturing of micro-robot in millimeter level in fields of micro bionic robots and medical robotics [17]. Therefore, it is possible to minimize the size of moving platform. The fixed base can also be scaled down through replacing existing actuators with smaller stepping motors with diameters to be within 4 mm, which can at least reduce the diameter of the entire bioprinter to be within 12 mm.

In terms of printing accuracy, the results of this experiment showed an average deviation of $1.18 \text{ mm} \pm 0.43 \text{ mm}$ in latticed structure and

0.67 mm \pm 0.15 mm in planar circle. Besides, it was found that the further the moving platform moved, the bigger the deviation was. This might be resulted from the width of the beams mentioned in the fabrication part was not strictly limited to 1 mm. Although the design principle was derived from PC-MEMS techniques, the manufacturing procedure was different. Standard procedure of PC-MEMS comprises the steps of additive lamination, subtractive micromachining, folding, and locking, which takes long and needs several processing equipment. In the fabrication of moving platform, no mechanical methods were used, which makes the fabrication efficient, low-cost but with a bit low accuracy. The width of the beams was slightly narrower than 1 mm and when the moving platform moved further away from the center, the deflection in the beam increased. Meanwhile, the narrow width prevented the deflection from increasing, making the deviations in the top view and side view both the largest. The deviation could be reduced by keeping the moving platform away from the front end of workspace. To achieve optimal manufacturing efficiency and printing accuracy in real applications, the fabrication method can be decided based on the size of printing targets.

The abstracted bioprinting process is basically the same as traditional extrusion bioprinting. But there still existed some differences that bioinks were extruded directly from a syringe to a nozzle driven by injection pump in common extrusion bioprinting, the nozzle is normally short and barely influence the bioink state [27]. During this bioprinting process, a long tube existed between the syringe and the nozzle, which might affect the state of bioinks. The shear stress during extrusion leads to decrease in viscosity of the bioinks due to their shear thinning property. In addition, heat generated by friction in the tube raised the temperature, which are all adverse to proper-gelation. Most of experiments using the parameter explored from our previous work would cause the bioinks in an under-gelation status owing to long-range shear stress as well as friction between the tubes. When the bioink was printed with an under-gelation status, it demonstrated droplet morphology at the nozzle tip and the bioink in a printed construct would fuse on the cross site, making it unfeasible to manufacture a 3D construct with mechanical strength.

Focusing on the issues above, numerous experiments were performed to find the optimal printing parameters and it turned out that extending the time syringe in the 4 °C refrigerator would be beneficial to gelation for its lower initial temperature. Most importantly, PTFE tube was used to replace common silicone tubes for its excellent lubricity. During extrusion, the shearing stress between fluid and tubes was caused by liquid slip on the solid surface at the micro level. And occurrence of slip depends whether solid surface can be wetted by the liquid. Compared with most of tubes, PTFE is hydrophobic and the

lower surface energy effect of PTFE tube makes it difficult to be wetted by hydrogel, which reduced viscous resistance in solid–liquid interface [28]. From a macro point of view, the flow resistance of liquid in cylindrical pipes was decided by fanning equation.

$$H_f = \frac{4\mu L}{D} \cdot \frac{V^2}{2g}$$

Where H_f represents the head loss caused by friction, μ represents the friction coefficient of tubes.

Owing to the smaller friction coefficient of PTFE tube compared with tube made with other materials [29], the friction during extrusion is much lower, which reduces the impact of shearing stress and heat generated by friction. As a consequence, it significantly increased the capacity of extrusion.

In bioprinting performance test, we demonstrate its printing feasibility through printing a 2-layer tissue scaffold containing GES-1 cells and HGSMCs to mimic the anatomical structure of stomach wall. However, there was a certain amount of residual bioinks in the tube after extrusion. Before the formal printing experiment, the volume of hydrogels needed in each layer was determined, after which the extrusion time for each layer can be calculated due to the constant extrusion speed. Based on this trial, the two different cell types were well separated in different layers in the final printed tissue scaffolds, which can be seen in figure 7.

In the selection of materials, numerous research studies from literature were performed to discuss the feasibility of alginate/gelatin hydrogels. As a well-developed biomaterial, alginate/gelatin hydrogels are widely used in 3D bioprinting including the epithelial cells [30] and smooth muscle cells [31] as the model cells in this study. In addition, former research studies have demonstrated that this material can adhere well on the targeted tissues in skin, bone, cartilage even stomach tissues [32–34]. Most bioprinting assumes a close to neutral pH environment, whereas the gastric tract is mostly acidic, which could impact the bioink hydrogels chemistry. Though no research has been done to verify the stability of alginate/gelatin structure in acid environment, the application of alginate/gelatin material in drug delivery can be used for reference. Researchers tend to get the drug released in intestinal tract rather than gastric tract for better absorption and related studies have shown that alginate/gelatin has the potential to shrink and become compact at low pH and can swell at high pH, which leads a slow release rate in gastric tract [35, 36]. It partly verified the stability of alginate/gelatin structures in acidic environment, but more exploration is still needed.

However, in view of the crosslinking mechanism, the ability to promote cell growth and toxicity of degradation products *in vivo*, alginate/gelatin material might not be the optimal choice for further development in the future. The core work of this paper is to come up with the concept of *in situ in vivo* bioprinting and verify the feasibility of the novel

micro bioprinter. As a consequence, the alginate/gelatin material was used in this preliminary research for its extensive sources and favorable printability. In addition, material requirements for extrusion are similar to those of other printing techniques, which in turn allows choosing from a wide range of biocompatible inks.

5. Conclusion

This paper proposed the concept of *in situ in vivo* bioprinting for the first time and verified the feasibility of this concept for treatment for gastric wall injuries. We present this work as a preliminary step towards a new method in the field of bioprinting. We have designed and fabricated a micro bioprinting platform which can be installed to an endoscope and we have also utilized this platform to print biomaterials hydrogels and human cells with high viability. PC-MEMS techniques were used in the design and fabrication of this platform, which makes it possible to carry out bioprinting in the micro scale. The platform printed the 2-layer tissue scaffolds in a stomach model and gelatin–alginate hydrogels with GES-1 and HGSMCs were used as bioink. The fabricated scaffolds showed good integrity and were observed for 10 d. LIVE/DEAD assay and cellular morphology observation suggested that the printed cells remained a high viability and a steady proliferation, which indicated good biological functions of the cells in printed scaffolds. This work presents an innovative advance not only in the field of bioprinting but also in clinical fields.

There are still some limitations in our preliminary research, in particular: (i) the outer diameter of the bioprinting platform is around 28 mm, which is a bit larger than the existing endoscope and thus places some limits in further animal experiments. Future iterations will utilize smaller actuators to minimize the size of the platform. (ii) The gelatin–alginate hydrogels only form stable structures at low temperatures and thus cannot form structures well in an animal's body (around 37 °C). Meanwhile, the cross-linking agent Ca^{2+} can influence the viability of cells during *in vivo* bioprinting [37]. New hydrogels system will be explored for *in situ in vivo* bioprinting. It should cross-link steadily in body temperature and be harmless to human cells. In addition, it should have favorable mechanical properties for bioprinting. (iii) The bioprinting platform is just a part of the *in situ in vivo* bioprinting system. The corresponding endoscope and other parts such as the detecting system will also be designed and integrated to make *in situ in vivo* bioprinting a reality.

Acknowledgments

This work was partially supported by the Key Research and Development Projects of Chinese People's Liberation Army (Grant No. BWS17J036).

ORCID iD

Tao Xu  <https://orcid.org/0000-0003-3685-0245>

References

- [1] Choudhury D, Tun H W, Wang T and Naing M W 2018 Organ-derived decellularized extracellular matrix: a game changer for bioink manufacturing? *Trends Biotechnol.* **36** 787–805
- [2] Gopinathan J and Noh I 2018 Recent trends in bioinks for 3D printing *Biomater. Res.* **22** 11
- [3] Murphy S V and Atala A 2014 3D bioprinting of tissues and organs *Nat. Biotechnol.* **32** 773–85
- [4] Lee V, Singh G, Trasatti J P, Bjornsson C, Xu X, Tran T N, Yoo -S-S, Dai G and Karande P 2013 Design and fabrication of human skin by three-dimensional bioprinting *Tissue Eng. Part C. Methods* **20** 473–84
- [5] Cui X, Breitenkamp K, Finn M, Lotz M and D'Lima D D 2012 Direct human cartilage repair using three-dimensional bioprinting technology *Tissue Eng. Part A* **18** 1304–12
- [6] Bendtsen S T, Quinnell S P and Wei M 2017 Development of a novel alginate-polyvinyl alcohol-hydroxyapatite hydrogel for 3D bioprinting bone tissue engineered scaffolds *J. Biomed. Mater. Res. A* **105** 1457–68
- [7] Campbell P G and Weiss L E 2007 Tissue engineering with the aid of inkjet printers *Expert Opin. Biol. Ther.* **7** 1123–7
- [8] Guillemot F *et al* 2010 High-throughput laser printing of cells and biomaterials for tissue engineering *Acta Biomater.* **6** 2494–500
- [9] Skardal A, Mack D, Kapetanovic E, Atala A, Jackson J D, Yoo J and Soker S 2012 Bioprinted amniotic fluid-derived stem cells accelerate healing of large skin wounds *Stem Cells Transl. Med.* **1** 792–802
- [10] Albanna M *et al* 2019 *In situ* bioprinting of autologous skin cells accelerates wound healing of extensive excisional full-thickness wounds *Sci. Rep.* **9** 1856
- [11] O'Connell C D *et al* 2016 Development of the biopen: a handheld device for surgical printing of adipose stem cells at a chondral wound site *Biofabrication* **8** 015019
- [12] Keriquel V, Guillemot F, Arnault I, Guillotin B, Miraux S, Amedee J, Fricain J-C and Catros S 2010 *In vivo* bioprinting for computer- and robotic-assisted medical intervention: preliminary study in mice *Biofabrication* **2** 014101
- [13] Vos T *et al* 2016 Global, regional, and national incidence, prevalence, and years lived with disability for 310 diseases and injuries, 1990–2015: a systematic analysis for the Global Burden of Disease Study 2015 *The Lancet* **388** 1545–602
- [14] Chen T, Lin Z-W, Zhang Y-Q, Chen W-F, Zhong Y-S, Wang Q, Yao L-Q, Zhou P-H and Xu M-D 2017 Submucosal tunneling endoscopic resection vs thoracoscopic enucleation for large submucosal tumors in the esophagus and the esophagogastric junction *J. Am. Coll. Surg.* **225** 806–16
- [15] Tan T M and Okada M 1999 The efficiency of absorbable clips in minimally invasive surgery *Surg. Today* **29** 828–31
- [16] Correa J E, Toombs J, Toombs N and Ferreira P M 2016 Laminated micro-machine: design and fabrication of a flexure-based Delta robot *J. Manuf. Process.* **24** 370–5

- [17] Sreetharan P S, Whitney J P, Strauss M D and Wood R J 2012 Monolithic fabrication of millimeter-scale machines *J. Micromech. Microeng.* **22** 055027
- [18] Pierrot F, Reynaud C and Fournier A 1990 DELTA: a simple and efficient parallel robot *Robotica* **8** 105–9
- [19] Vischer P and Clavel R 1998 Kinematic calibration of the parallel Delta robot *Robotica* **16** 207–18
- [20] Stock M and Miller K 2003 Optimal kinematic design of spatial parallel manipulators: application to linear delta robot *J. Mech. Des.* **125** 292–301
- [21] Bonev I 2001 'Delta parallel robot-the story of success' Newsletter www.parallelmic.org
- [22] Fritsch F N and Carlson R E 1980 Monotone piecewise cubic interpolation *SIAM J. Numer. Anal.* **17** 238–46
- [23] Laribi M, Romdhane L and Zeghloul S 2007 Analysis and dimensional synthesis of the Delta robot for a prescribed workspace *Mech. Mach. Theory* **42** 859–70
- [24] Liebermann-Meffert D M, Meier R and Siewert J R 1992 Vascular anatomy of the gastric tube used for esophageal reconstruction *Ann. Thorac. Surg.* **54** 1110–5
- [25] Ke Y, Ning T and Wang B 1994 Establishment and characterization of a SV40 transformed human fetal gastric epithelial cell line-GES-1 *Zhonghua Zhong Liu Za Zhi* **16** 7–10
- [26] Patel N, Darzi A and Teare J 2015 The endoscopy evolution: 'the superscope era' *Frontline Gastroenterol.* **6** 101–7
- [27] Ouyang L, Yao R, Zhao Y and Sun W 2016 Effect of bioink properties on printability and cell viability for 3D bioplotting of embryonic stem cells *Biofabrication* **8** 035020
- [28] Qi H, Liang A, Jiang H, Chong X and Wang Y 2018 Effect of pipe surface wettability on flow slip property *Ind. Eng. Chem. Res.* **57** 12543–50
- [29] Biswas S and Vijayan K 1992 Friction and wear of PTFE—a review *Wear* **158** 193–211
- [30] Singh D, Zo S M, Kumar A and Han S S 2013 Engineering three-dimensional macroporous hydroxyethyl methacrylate-alginate-gelatin cryogel for growth and proliferation of lung epithelial cells *J. Biomater. Sci. Polym. Ed.* **24** 1343–59
- [31] Baniasadi H, Mashayekhan S, Fadaoddini S and Haghsharifarizamini Y 2016 Design, fabrication and characterization of oxidized alginate–gelatin hydrogels for muscle tissue engineering applications *J. Biomater. Appl.* **31** 152–61
- [32] Balakrishnan B, Joshi N, Jayakrishnan A and Banerjee R 2014 Self-crosslinked oxidized alginate/gelatin hydrogel as injectable, adhesive biomimetic scaffolds for cartilage regeneration *Acta Biomater.* **10** 3650–63
- [33] Xia Y, Mei F, Duan Y, Gao Y, Xiong Z, Zhang T and Zhang H 2012 Bone tissue engineering using bone marrow stromal cells and an injectable sodium alginate/gelatin scaffold *J. Biomed. Mater. Res. A* **100** 1044–50
- [34] Joddar B, Tasnim N, Thakur V, Kumar A, McCallum R W and Chattopadhyay M 2018 Delivery of mesenchymal stem cells from gelatin–alginate hydrogels to stomach lumen for treatment of gastroparesis *Bioengineering* **5** 12
- [35] Khandai M, Chakraborty S, Nayak P, Bala Murali Krishna N, Chakravarthi G, Acharjya B and Kumar Ghosh A 2012 Preparation and *in vitro in vivo* evaluation of aceclofenac loaded alginate microspheres: an investigation of effects of polymer using multiple comparison analysis *Curr. Drug. Deliv.* **9** 495–505
- [36] Mohammadi M, Heshmati M K, Sarabandi K, Fathi M, Lim L-T and Hamishehkar H 2019 Activated alginate-montmorillonite beads as an efficient carrier for pectinase immobilization *Int. J. Biol. Macromol.* **137** 253–60
- [37] Khalil S and Sun W 2009 Bioprinting endothelial cells with alginate for 3D tissue constructs *J. Biomech. Eng.* **131** 111002